Nano Today 38 (2021) 101144

Contents lists available at ScienceDirect

Nano Today

journal homepage: www.elsevier.com/locate/nanotoday

Radionuclide labeled gold nanoclusters boost effective anti-tumor immunity for augmented radio-immunotherapy of cancer

Pei Pei, Wenhao Shen, Hailin Zhou, Yuanchen Sun, Jing Zhong, Teng Liu, Kai Yang*

State Key Laboratory of Radiation Medicine and Protection, School of Radiation Medicine and Protection & School for Radiological and Interdisciplinary Sciences (RAD-X), Collaborative Innovation Center of Radiation Medicine of Jiangsu Higher Education Institutions, Soochow University, Suzhou, Jiangsu 215123, China

ARTICLE INFO

Article history:
Received 22 November 2020
Received in revised form 23 February 2021
Accepted 25 March 2021
Available online xxxx

Keywords:
Gold nanocluster
Radionuclides
Spontaneously metastatic tumors
Radio-immunotherapy

ABSTRACT

Given the complexity, heterogeneity and metastasis of patient tumors, the combined therapy is usually applied in clinical applications. Internal radioisotope therapy has been an indispensable treatment strategy for primary tumor nowadays. However, the therapeutic effect of internal radioisotope therapy is dissatisfactory for distant tumors or spontaneously metastatic tumors. Herein, we design radionuclide labelled glutathione modified gold nanoclusters (technetium-99m labelled gold nanoclusters (^{99m}Tc@Au NCs) and lutecium-177 labelled gold nanoclusters (^{177}Lu@Au NCs)) by simple chelation between glutathione and radionuclide. Such radionuclide labelled gold nanoclusters could not only enhance the therapeutic outcomes of internal radioisotope therapy but also induce anticancer immunity by activation of dendritic cells (DCs). In addition, ^{177}Lu@Au NCs could effectively eliminate primary tumors and suppress the growth of distant tumors when combined with immune checkpoint inhibitors. Furthermore, a long-term immunological memory effect is also observed after internal radioisotope therapy. Importantly, on a clinical-relevant transgenic mice model, we for the first time use such therapeutic strategy to significantly suppress the growth of spontaneously metastatic tumors and lengthen the survival time of the transgenic mice. Our study presents a novel approach for tumor radio-immunotherapy and meanwhile provides a new idea for spontaneously metastatic tumors in clinic.

Introduction

The death of tumor patients is often caused by tumor metastasis, rather than the primary tumor [1–3]. Therefore, how to achieve solid tumor treatment and inhibit tumor metastasis is a key point in the field of clinical treatment [4,5]. For patients with cancer at an early stage, the use of imaging technology, tumor markers and other biologic methods to achieve the early lesion detection and timely scientific treatment are beneficial for radical treatment [6–8]. For advanced stages of cancer especially metastatic tumors, however, it is hard to achieve effective radical cure [9,10]. The current clinical treatment methods for spontaneously metastatic tumors include chemotherapy, molecular targeted therapy or combined therapy, *etc.* [11–17]. Unfortunately, the systemic side effects and nonspecific distribution further limit the therapeutic efficacy of those therapeutic modalities in a certain extent [18–20]. With the blooming of cancer immunotherapy in recent years, which can train the immune system of patients to assault distant or metastatic tumors and produce a certain immune memory effect, tumor treatment strategies are further expanded [21,22]. In immunotherapies for cancer, the use of immune checkpoint inhibitors such as anti-PD1/anti-PD-L1 or anti-CTLA-4 has achieved inspiring clinical effects in curing of some specific tumors [23–25]. Nevertheless, the response rate of immunotherapy is still relatively low for patients with tumor, which less than 30% on average. In order to further improve the response rate of immunotherapy, chemotherapy, radiotherapy or other treatments, which can induce the immunogenic cell death of tumor cells and enhance tumor immunogenicity, are also applied to combine with immune checkpoint inhibitors [26,27]. Among them, radiation therapy (RT) including external beam radiotherapy (EBRT) and internal radioisotope therapy have been indispensable treatments strategy in clinical trials [28–30]. However, the therapeutic effect of radiotherapy, especially internal radioisotope therapy, is still restricted by some certain mechanisms, such as off-targeted radionuclides, physiological toxicity and radiation resistance caused by tumor hypoxic microenvironment [31,32].

With the flourishing development of nanotechnology, nanomedicine strategies have been applied to improve the efficacy of

* Corresponding author.
E-mail address: kyang@suda.edu.cn (K. Yang).

https://doi.org/10.1016/j.nantod.2021.101144
1748-0132/

internal radioisotope therapy in last decades. Numerous stabilized nanocarriers have been applied to transport therapeutic radioisotopes to tumor sites for internal radioisotope therapy either alone or combined with other types of therapies [33–35]. In addition, various functional nanomaterials also have been developed to modulate the microenvironment of solid tumors to surmount hypoxia-associated radiation resistance and enhance RT efficacy [36–38]. Among them, gold nanomaterials are most widely used in the field of radiotherapy due to their High-Z elements to deposit radiation energy as well as their excellent biocompatibility with little toxicity concern. The different radioisotopes including $^{123/124/125/131}$I, ^{64}Cu, ^{68}Ga, ^{198}Au, ^{99m}Tc and ^{111}In have been labelled on gold nanomaterials *via* different strategies [39–42]. In recent work, ^{131}I labeled gold nanoparticles with PEG modification have been reported for nuclei-targeting internal radio-immunity therapy [48]. However, those labeling strategies often require additional chelating agents, linkers or harsh conditions, which may affect the size or surface properties of gold nanomaterials, and further alter the *in vivo* behaviors of gold nanomaterials [43,44]. It is necessary to develop simple and easy-to-use radionuclide-labelled gold nanoparticles for cancer internal radioisotope therapy. Gold nanoclusters with ultra-small sizes, which could be eliminated by the kidneys, have shown enormous potential in clinical imaging and treatment. Meanwhile, many challenges in their clinical translation should be addressed [45–47]. Therefore, the development of radionuclide labelled gold nanocluster by a simple and easy method may blaze a new path for internal radioisotope therapy based on gold nanomaterials.

In this work, glutathione modified gold nanoclusters (GSH-Au NCs) were synthesised by chemical reduction of $HAuCl_4$ with glutathione. The obtained GSH-Au NCs could be further loaded with diagnostic radioisotope ^{99m}Tc (half-life of 6.02 h) and therapeutic radioisotope ^{177}Lu (half-life of 6.71 d) with high efficiency by simple chelation (Fig. 1a). Interestingly, ^{99m}Tc@Au NCs could not only act as an imaging platform to exhibit *in vivo* behaviour, but also serve as a radiosensitizer to endow nontherapeutic ^{99m}Tc with therapeutic function by absorbing γ rays and emitting charged particles. However, the therapeutic effect of ^{99m}Tc@Au NCs was confined by the short half-time of ^{99m}Tc. Remarkably, by conveniently chelating therapeutic radioisotope (^{177}Lu) with carboxyl group on the surface of GSH-Au NCs, ^{177}Lu@Au NCs could tremendously improve the internal radioisotope therapy efficacy of ^{177}Lu compared with free ^{177}Lu. Furthermore, immunogenic cell death (ICD) of cancer cells induced by internal radioisotope therapy could activate various immune cells and unregulated the expression of PD-L1 on tumor cells, which showed great synergy with anti-PD-L1 (αPD-L1) blockade in suppressing distant tumors and providing a long-term immune memory protection for the treated mice (Fig. 1b). More importantly, such therapeutic strategy even exhibited an amazing therapeutic effect for the spontaneously metastatic tumors, achieving remarkable enhancement in survival quality and lifetime of transgenic mice. This novel approach for radio-immunotherapy presented by us would provide more opportunities and time for clinical treatment of spontaneously metastatic tumors.

Results and discussion

Enhanced internal radioisotope therapy by radionuclide labelled Au NCs

The GSH-Au NCs were synthesized by a chemical reduction method according the published protocols[46]. The Fourier Transform Infrared Spectroscopy (FTIR) spectra of GSH-Au NCs showed that the peak at 2522 cm^{-1} of GSH corresponding to S-H stretching vibration mode disappeared after reaction, indicating the successful synthesis of GSH-Au NCs (Fig. 1c). Transmission electron microscope (TEM) image revealed that the size of GSH-Au NCs was ~2.5 nm (Fig. 1d), which was also verified by dynamic light scattering (DLS) (Fig. 1f). The absorption and fluorescence spectra of GSH-Au NCs exhibited that the maximum emission and excitation peaks were at 835 nm and at 410 nm respectively (Fig. 1e). Afterwards, with excellent stability in PBS and serum (Fig. S1), GSH-Au NCs was further applied to label with two different radionuclides including ^{99m}Tc (a diagnostic radioisotope emitting γ rays (140 keV)) and ^{177}Lu (a therapeutic radioisotope emitting β particles (497 keV)) with high radiolabelling yield (67.17% and 90.74%) respectively by simple chelation. Because of moderate reaction conditions, the size of GSH-Au NCs (~2.5 nm) almost unchanged after radiolabelling (Fig. 1f). Furthermore, the characterization of UV, Raman spectroscopy and Zeta potential also showed that the radiolabeling would not affect the morphology and optical properties of GSH-Au NCs (Fig. S2). Notably, both radionuclides ^{99m}Tc and ^{177}Lu labelled GSH-Au NCs exhibited excellent radiostability in PBS and serum at 37 °C of incubation through radiolabelling stability assay (Fig. 1g), which was favourable for the following *in vitro* and *in vivo* studies. Gold, as a High-Z element, could interact with X-rays or γ rays to produce secondary charged particles, which would further deposit high energy in tumor cells and enhance therapeutic efficiency of radiotherapy. Radioisotope ^{99m}Tc is widely used as contrast agent for SPECT/CT imaging in clinic, while it could not emit alpha (α), beta (β) or auger particles for radiotherapy. In order to testify the radiosensitization ability of ^{99m}Tc@GSH-Au NCs, liquid scintillation spectroscopy has been used to detect the generation of charged secondary particles from ^{99m}Tc@Au NCs. As shown in the Fig. 1h, ^{99m}Tc@Au NCs exhibited stronger peak than that of free radionuclide, indicating the effective production of charged secondary particles from ^{99m}Tc@Au NCs, which might endow nontherapeutic ^{99m}Tc with therapeutical effect.

Encouraged by the superior property of our design, the *in vitro* internal radioisotope therapy therapeutic function of ^{99m}Tc@Au NCs and ^{177}Lu@Au NCs were then evaluated through a series of experiments. Owing to favourable modified by glutathione, GSH-Au NCs exhibited superior biocompatibility with different cells even at high concentrations (Au: 160 μg/mL) (Fig. 2a). On the contrary, 4T1 cells treated with ^{99m}Tc@Au NCs and ^{177}Lu@Au NCs revealed lower cell viability with the increase of the radioactive dose (Fig. 2b). Especially when radioactive dose of ^{177}Lu@Au NCs just reached 10 μCi, the relative cell viability of 4T1 was rapidly decreased to 11.15 ± 2.94%. Furthermore, Au NCs labelled with nontherapeutic ^{99m}Tc also displayed visible cytotoxicity for 4T1 cells, which profited from radiosensitization and enhanced uptake of GSH-Au NCs (Figs. 2c and S3). Notably, directly exposing cells to free ^{99m}Tc or free ^{177}Lu indicated that there was no obvious toxicity to cancer cells, demonstrating the little internal radioisotope therapy efficiency of free ^{99m}Tc and free ^{177}Lu. Afterwards, we further confirmed the internal radioisotope therapy capacity of ^{99m}Tc@Au NCs and ^{177}Lu@Au NCs by clonogenic assay (Fig. 2d). According to the cell survival fraction curves, the surviving fragments, which were calculated by the ratio of surviving colonies and seeded cells, of ^{99m}Tc@Au NCs and ^{177}Lu@Au NCs were much less than free radionuclides. Generally, radioisotopes used in internal radioisotope therapy could emit energy from the nucleus, generating ionized atoms and free radicals to cause the double-strand cleavages in DNA, which would further induce cell apoptosis. To evaluate double-strand DNA damages of tumor cells treated by internal radioisotope therapy, 4T1 cells were firstly incubated with ^{99m}Tc@Au NCs or ^{177}Lu@Au NCs at different radioactive dose (^{99m}Tc: 300 μCi, ^{177}Lu: 10 μCi, Au: 160 μg/mL) and then stained with γ-H2AX, a frequently-used marker for DNA breaks. As indicated in Fig. 2e, the cells treated with ^{99m}Tc@Au NCs exhibited visible red fluorescence. The similar situation was also observed in ^{177}Lu@Au NCs group, but the fluorescence signal was stronger than that of ^{99m}Tc@Au NCs. In contrast, the cells treated with free radioisotopes and GSH-Au NCs showed few or no red fluorescence, which was strongly in line with our expectations. Therefore, the strategies of labeling radionuclides on GSH-Au NCs could not only improve the internal radioisotope

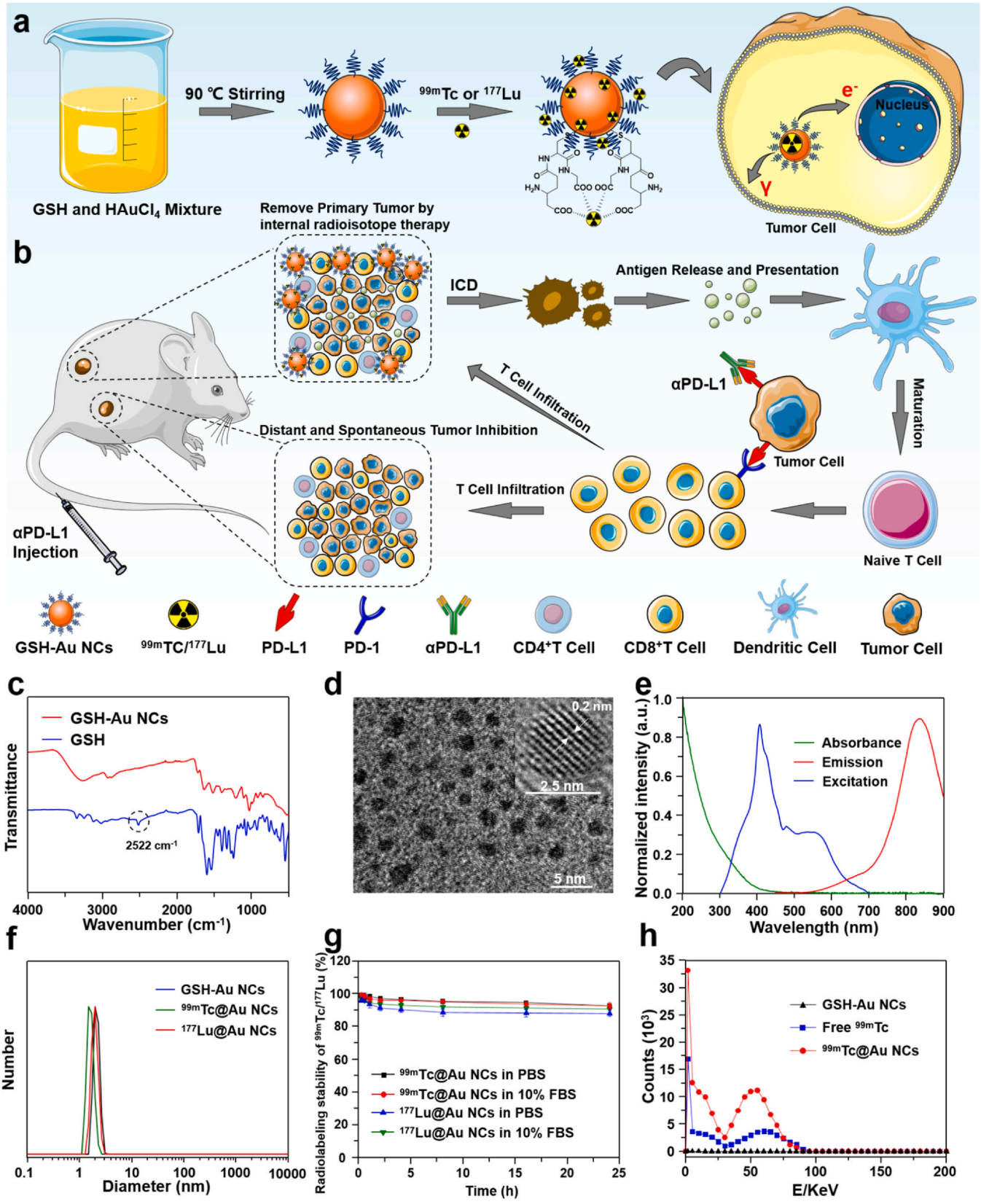

Fig. 1. The schematic diagram of our design and characterization of Au NCs. a) Synthetic procedure of radionuclide labelled Au NCs. b) The mechanism of antitumor immune responses induced by radionuclide labelled Au NCs in combination with checkpoint-blockade to inhibit distant and spontaneous tumors. c)TEM images of GSH-Au NCs. d) FT-IR spectra of glutathione and purified GSH-Au NCs. e) UV–vis and fluorescence spectra of GSH-Au NCs. f) DLS of GSH-Au NCs, ^{99m}Tc@Au NCs and ^{177}Lu@Au NCs. g) Radiolabeling stability of ^{99m}Tc@Au NCs and ^{177}Lu@Au NCs in PBS and serum. h) The liquid scintillation spectrum of free ^{99m}Tc, GSH-Au NCs, and ^{99m}Tc@Au NCs.

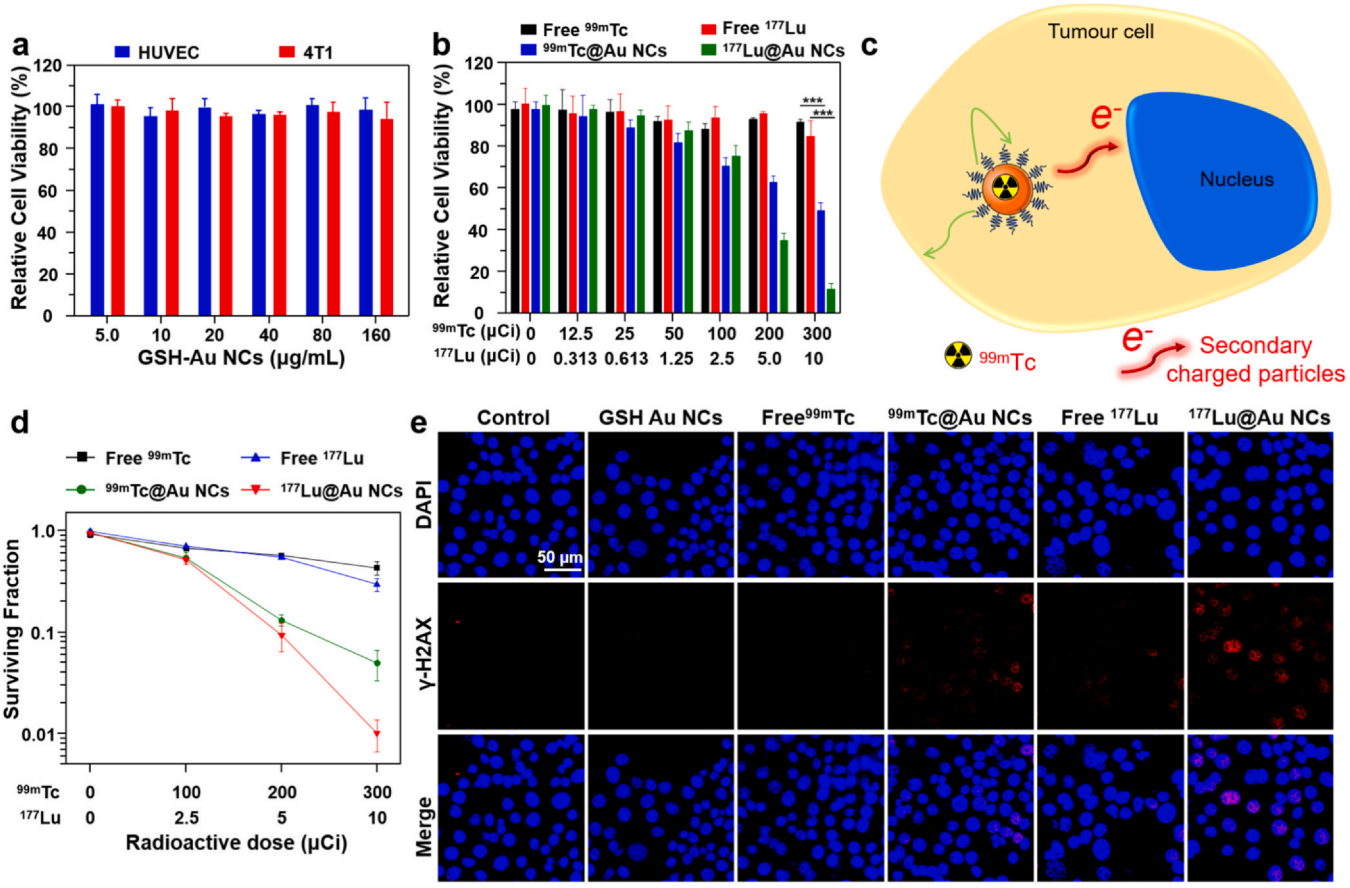

Fig. 2. *In vitro* internal radioisotope therapy by ^{99m}Tc@Au NCs and ^{177}Lu@Au NCs. a) Cytotoxicity of GSH-Au NCs at different concentrations. b) Relative viabilities of 4T1 cells treated with free ^{99m}Tc, free ^{177}Lu, ^{99m}Tc@Au NCs and ^{177}Lu@Au NCs with different doses for 24 h. c) The self-sensitization effect by ^{99m}Tc@Au NCs to destruct tumor cells. d) Colongenic assay of 4T1 cells treated by free ^{99m}Tc, free ^{177}Lu, ^{99m}Tc@Au NCs and ^{177}Lu@Au NCs at different doses. e) γ-H2AX fluorescence images (blue: DAPI, red: γ-H2AX) of 4T1 cells 24 h after different treatments (Control, GSH-Au NCs, free ^{99m}Tc, free ^{177}Lu, ^{99m}Tc@Au NCs and ^{177}Lu@Au NCs). P values in (c) were calculated by multiple *t*-tests (***P < 0.001).

therapy of therapeutic radioisotope ^{177}Lu, but also endow non-therapeutic ^{99m}Tc with the therapeutic function through absorbing γ rays to emit the charged particles.

On account of the high therapeutic efficiency in the *in vitro* level, we further explored *in vivo* behaviours of radionuclide labelled Au NCs. Firstly, we explored the tumor retention ability of ^{99m}Tc@Au NCs after local injection into the tumor. 4T1 tumor-bearing mice were intratumorally (i.t.) injected with free ^{99m}Tc, ^{99m}Tc@Au NCs at radioactive dose of 800 μCi or free ^{177}Lu, ^{177}Lu@Au NCs at radioactive dose of 100 μCi and SPECT/CT images were collected at different time points post injection. It was distinctly observed that free ^{99m}Tc was quickly metabolized to other normal organs from tumor site just after 1 h of injection. Conversely, ^{99m}Tc@Au NCs exhibited a long retention in tumor site and a little distribution in normal organs even after 24 h of injection. Similarly, ^{177}Lu@Au NCs also visibly enhanced the retention time of radionuclides in the tumor sites compared to free ^{177}Lu (Figs. 3a and S4). Moreover, *ex vivo* biodistribution studies were simultaneously carried out by testing radioactivity of major organs and tumors though γ counter at 24 h post-injection. The results showed that the i.t. injection of ^{99m}Tc@Au NCs could significantly enhance the retention of radionuclide in tumor site and reduce the distribution of radionuclide in normal tissues (Fig. 3b), which is favourable for internal radioisotope therapy *in vivo*. In addition, the tumor homing ability of ^{99m}Tc@Au NCs by intravenous (i.v.) injection was also evaluated. Mice bearing 4T1 tumor were i.v. injected with ^{99m}Tc@Au NCs and scanned by SPECT/CT images at different time points post injection. SPECT/CT images indicated that ^{99m}Tc@Au NCs could effectively accumulate in tumor site by enhanced permeability and retention effect (Fig. S5a). The consequence of SPECT/CT images were further testified by biodistribution data of mice, which correlated well with the results of SPECT/CT images (Fig. S5b). In addition, the pharmacokinetic parameters of GSH-Au NCs and ^{99m}Tc@Au NCs were measured in normal BALB/c mice, and showed that both GSH-Au NCs and ^{99m}Tc@Au NCs could prolong blood circulation time after i.v. injection (Fig. S5c). Generally, by SPECT/CT imaging and *ex vivo* biodistribution studies, we found that such radionuclide labelled Au NCs only distributed in tumors and bladder after i.t. injection, which may afford effective internal radioisotope therapy with low physiological toxicity.

Inspired by the superior distribution in tumor site, we then evaluated the internal radioisotope therapy efficacy of radionuclide labelled Au NCs for local tumors. In details, BALB/c mice bearing 4T1 murine breast tumors were assigned into seven groups at random (n = 5 per group) (Fig. 3c). (Group 1, PBS; Group 2, GSH-Au NCs (i.v.); Group 3, GSH-Au NCs (i.t.); Group 4, free ^{99m}Tc (i.t., 200 μCi); Group 5, Free ^{177}Lu (i.t., 75 μCi); Group 6, ^{99m}Tc@Au NCs (i.v., 400 μCi); Group 7, ^{177}Lu@Au NCs (i.v., 200 μCi); Group 8, ^{99m}Tc@Au NCs (i.t., 200 μCi); Group9, ^{177}Lu@Au NCs (i.t., 75 μCi). When the volume of tumors reached ~100 mm^3, mice were injected with the corresponding formulations by i.v. or i.t. injection. Compared to GSH-Au NCs, free ^{99m}Tc and free ^{177}Lu, which exhibited no obvious tumor growth inhibition effect, tumors treated by ^{99m}Tc@Au NCs and ^{177}Lu@Au NCs with i.t. or i.v. injection showed significantly suppression for tumor growth, in particular, tumor growth was almost completely suppressed by i.t. injection with ^{177}Lu@Au NCs only at 75 μCi. Furthermore, mice were sacrificed at 14 d post various

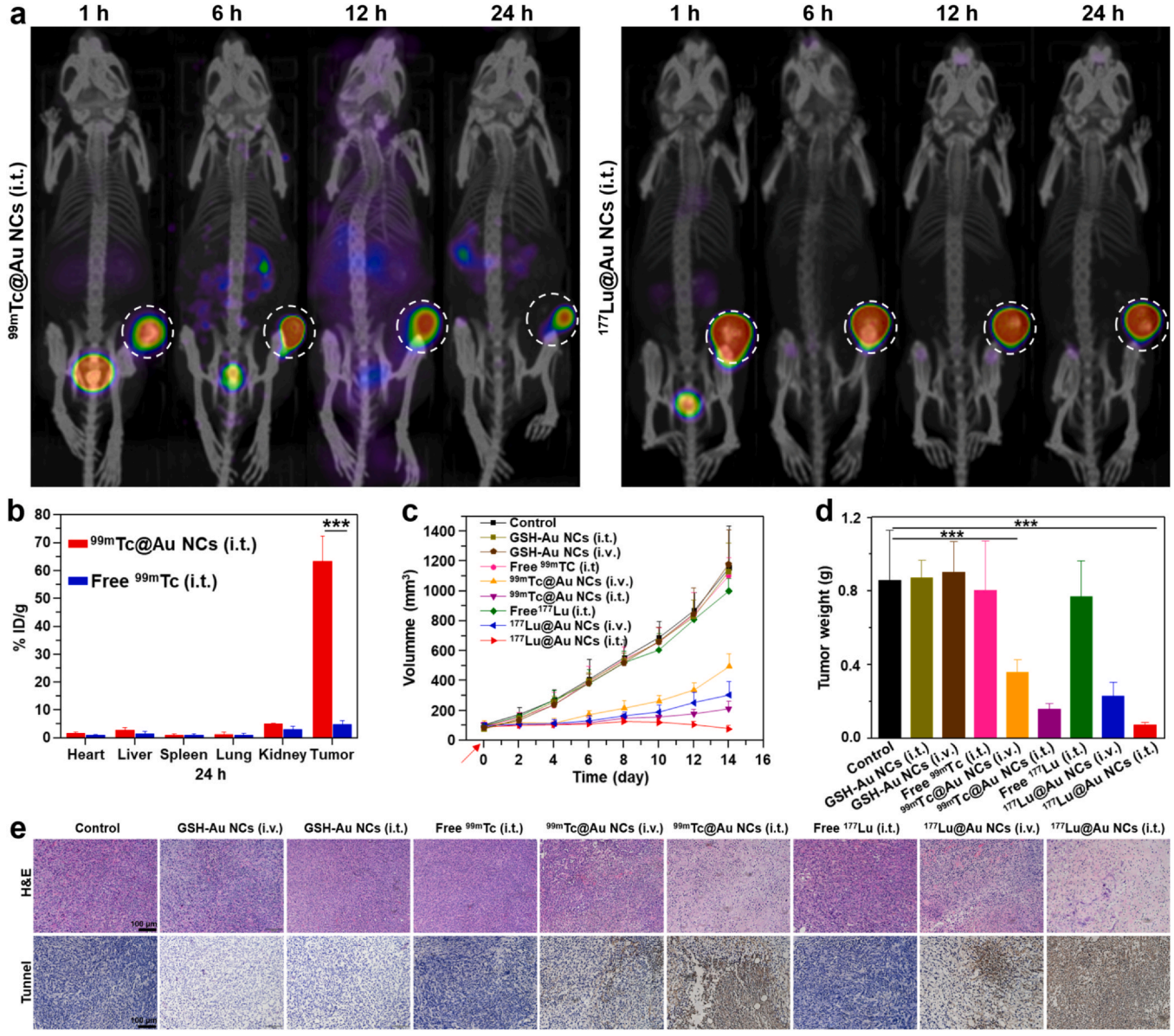

Fig. 3. *In vivo* biodistribution and internal radioisotope therapy based on ^{99m}Tc@Au NCs and ^{177}Lu@Au NCs. a) SPECT/CT images of 4T1 tumor-bearing mice post i.t. injection of ^{99m}Tc@Au NCs and ^{177}Lu@Au NCs. b) Biodistribution of free ^{99m}Tc, ^{99m}Tc@Au NCs in mice at 24 h post i.t. injection. Error bars represent mean ± s.d. (n = 3). c) Tumor growth curves of mice after the treatment by GSH-Au NCs (i.v.), GSH-Au NCs (i.t.), free ^{99m}Tc (i.t., 200 μCi), free ^{177}Lu (i.t., 75 μCi), ^{99m}Tc@Au NCs (i.v., 400 μCi), ^{177}Lu@Au NCs (i.v., 200 μCi), ^{99m}Tc@Au NCs (i.t., 200 μCi) or ^{177}Lu@Au NCs (i.t., 75 μCi). d) Average tumor weights of different groups collected 14 days after various treatments. Error bars represent mean ± s.d. (n = 5). e) Micrographs of H&E and TUNEL stained tumor slices from mice collected 3 days after the first treatment. P values in (b) and (d) were calculated by multiple *t*-tests (***P < 0.001).

treatments to collect data of tumor weights, which also demonstrated the effective radio-therapeutic effect of such radionuclide labelled Au NCs (Fig. 3d). Afterwards, hematoxylin & eosin (H&E) staining and terminal deoxynucleotidyl transferase dUTP nick end labelling (TUNEL) assay were carried out to evaluate morphologic changes and apoptosis of tumor cells at 3 day post various treatments. As shown in Fig. 3e, the most remarkable cell damage and apoptosis were observed in tumors treated with ^{177}Lu@Au NCs (i.t., 75 μCi), and a similar situation was also observed in ^{99m}Tc@Au NCs (i.t., 200 μCi). In terms of the potential side effects, body weights were monitored during internal radioisotope therapy and no significant changes were found in the body weight of the mice injected with ^{99m}Tc@Au NCs or ^{177}Lu@Au NCs (Fig. S6). Meanwhile, histological examination of main organs for mice by H&E staining also indicated no significant side effects of such radionuclide labelled Au NCs based-internal radioisotope therapy (Fig. S7).

Immune responses triggered by radionuclide labelled Au NCs

It has been discovered that ablative treatment methods, such as chemotherapy, photothermal therapy and radiotherapy, for tumors could induce tumor specific immune responses by generating tumor-associated antigens. Therefore, we investigated the immunological responses after the internal radioisotope therapy ablation of colorectal cancer CT26 tumors by radionuclide labelled Au NCs. Usually, antigen-presenting cells (APCs) such as DCs are able to capture and process antigens to activate T cells and trigger subsequent immune responses. As a consequence, the maturation of DCs is a critical initial step to initiate immunotherapy. In order to study *in vivo* DC activation by internal radioisotope therapy, lymph gland was obtained from the ipsilateral inguinal of each CT26 tumor-bearing mouse 3 days after different treatments (surgery, free ^{99m}Tc, ^{177}Lu, ^{99m}Tc@Au NCs, ^{177}Lu@Au NCs, n = 4 per

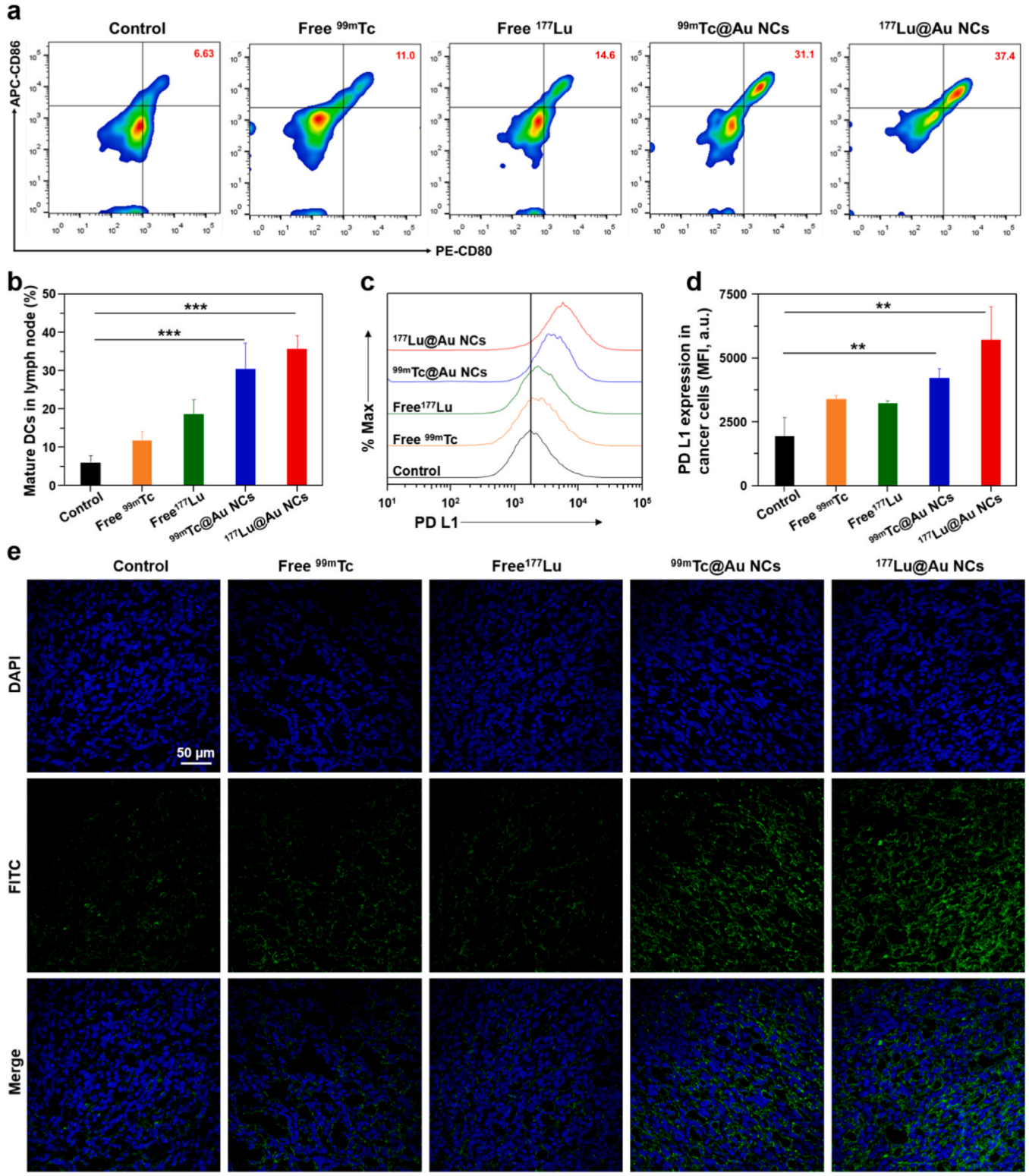

Fig. 4. Immune responses after treatment with radionuclide labelled Au NCs. a) and b) FACS plots (a) and statistic data (b) of DC maturation induced by radionuclide labelled Au NCs on mice bearing CT26 tumors. Lymph nodes cells were collected 3 days after treatments and assessed by flow cytometry after stain with CD11c, CD80 and CD86. Error bars represent mean ± s.d. (n = 4). c) and d) Representative histograms (c) and statistic data (d) of PD-L1 expression on CT26 cells isolated from distant tumors 3 days after treatment. Error bars represent mean ± s.d. (n = 4). e) The immunofluorescence slices of the PD-L1 expression in distant tumors (blue: DAPI, green: PD-L1). P values in (b) and (d) were calculated by multiple *t*-tests (***P < 0.001, **P < 0.01).

group) by i.t. injection for flow cytometry assay. Compared to the control group, both ^{99m}Tc@Au NCs and ^{177}Lu@Au NCs could prominently induce the DC maturation (~30.4% and ~35.65% respectively) *in vivo*, while free radionuclides showed negligible DC maturation stimulation effect (Fig. 4a and b). Therefore, the internal radioisotope therapy treatment of tumor by radionuclide labelled Au NCs may act as an immunostimulant to reinforce the immune responses post therapy.

The immunoregulation capability of internal radioisotope therapy were then tested in a distant tumor model by testing their expression of PD-L1. In details, the first tumor was treated by i.t. injection of free radionuclides (free ^{99m}Tc, ^{177}Lu) or radionuclide labelled Au NCs (^{99m}Tc@Au NCs, ^{177}Lu@Au NCs), and the other side tumor was harvested to evaluate the expression of PD-L1 by flow cytometry assay. To our surprise, PD-L1 expression on the distant tumors of mice treated by ^{99m}Tc@Au NCs or ^{177}Lu@Au NCs groups both exhibited a certain increase compared to other groups (Fig. 4c and d). To further demonstrate the results, the distant tumors were harvested for immunofluorescence staining analysis after various treatment of local tumors. Notably, it was found that the expression of PD-L1 represented by the FITC were significantly enhanced in the tumor of mice injected with ^{99m}Tc@Au NCs or ^{177}Lu@Au NCs compared to other groups (Fig. 4e). We speculated that such a phenomenon may be due to the immunogenic death of cancer cells caused by internal radioisotope therapy further promoting the tumor immune response. In order to avoid the attack of effector T cells, the remote tumors will increase the expression of PD-L1 to escape the killing of immunoreaction. Therefore, such effective internal radioisotope therapy not only promoted the maturation of DCs, but also up-regulated the expression of PD-L1 on distant tumors. In order to further enhance the anti-tumor effect for distant tumors and spontaneously metastasizing tumors, αPD-L1 was further combined with radionuclide labelled Au NCs for radio-immunotherapy of cancer.

Combined internal radioisotope therapy with immunotherapy to inhibit the distant tumors

Cancer immunotherapy has been developed rapidly in recent years, which could activate the body's initial immune system to attack metastatic tumor cells. Among them, immune checkpoint inhibitors such as αPD-L1 and anti-CTLA-4 (αCTLA-4) have shown inspiring clinical results for certain types of cancer. Therefore, distant tumor model was built to explore the combination of internal radioisotope therapy enhanced by radionuclide labelled Au NCs together with αPD-L1 blockade therapy. In details, 4T1 cells or CT26 cells were inoculated on the two sides of the back of each BALB/c mouse. When the volume of both tumors reached ~75 mm^3, mice were assigned at random into 6 groups (n = 5 per group) (Group 1, surgery; Group 2, surgery plus αPD-L1; Group 3, ^{99m}Tc@Au NCs (i.t.); Group 4, ^{177}Lu@Au NCs (i.t.); Group 5, ^{99m}Tc@Au NCs (i.t.) plus αPD-L1; Group 6, ^{177}Lu@Au NCs (i.t.) plus αPD-L1) and right flank tumors were removed by internal radioisotope therapy or surgery. Mice in Group 2, Group 5 and Group 6 were then i.v. injected with αPD-L1 (20 μg per mouse) at 1, 3 and 5 days. Afterwards, the growth of left flank tumors was monitored every two days (Fig. 5a). For 4T1 tumor model, the growth of the distant tumors on mice whose first tumors were i.t. injected with ^{99m}Tc@Au NCs or ^{177}Lu@Au NCs alone showed no significant difference from the surgery group. However, the treatment of ^{99m}Tc@Au NCs or ^{177}Lu@Au NCs plus αPD-L1 showed obvious growth inhibition on the distant tumors and effectively prolonged the lifetime of mice (Fig. 5b and c). Similar to the 4T1 tumor model, mice bearing CT26 tumors treated with αPD-L1 blockade plus internal radioisotope therapy with ^{99m}Tc@Au NCs also revealed a remarkable growth inhibition of the distant tumors. It was noteworthy noting that for the mice whose primary tumor was eliminated by ^{177}Lu@Au NCs and further blocked by αPD-L1, most of the distant tumors disappeared and 4 out of 5 mice could survive more than 60 days in this group (Fig. 5d and e). Meanwhile, the body weights were monitored during radio-immunotherapy and no appreciable body weight changes of mice were found, indicating such treatment strategy with no significant side effects for mice (Fig. S8a and b).

Additionally, the mechanisms of antitumor immune responses after combined radio-immunotherapy with radionuclide labelled Au NCs were further explored. Firstly, to assess the immune cells in distant CT26 and 4T1 tumors at day 10 post internal radioisotope therapy, tumors were harvested from mice receiving different treatments to evaluate the ratio of CD8 + cytotoxic T lymphocytes (CTLs) by flow cytometry assay. Interestingly, it was found that the percentage of CTLs showed great increase in combination of internal radioisotope therapy with αPD-L1 treated groups (*e.g.* Group 5 and Group 6) compared to other groups (Fig. 5f and g). Especially for mice treated by ^{177}Lu@Au NCs plus αPD-L1, the percentage of CTLs was up to 53.45%. A similar situation could also be seen in the 4T1 tumor model, the percentage of CTLs in mice treated with ^{177}Lu@Au NCs plus αPD-L1 increased to 41.93% compared to control group (18.25%) (Fig. S9a and b). Furthermore, tumor necrosis factor (TNF-α) and interferon gamma (IFN-γ), which play important roles in the cytotoxic functions of CTLs, in serum of mice were also analysed by ELISA kits at the same time. As shown in Fig. 5h and i, both TNF-α and IFN-γ showed obvious increase in ^{177}Lu@Au NCs plus αPD-L1 group, which further proved the inhibitory effect of radio-immunotherapy on distant tumors by our strategy. All those results strongly indicated that internal radioisotope therapy by ^{177}Lu@Au NCs combined with αPD-L1 would induce systemic anti-tumor immune responses to inhibit the growth of distant tumors, which is promising for inhibiting of spontaneously metastasizing tumors.

Internal radioisotope therapy plus immunotherapy to prevent tumor recurrence

Immunological memory could enable the immune system to protect organisms from a second wave of pathogen infection including cancer cells. In order to investigate immune memory effect triggered by ^{177}Lu@Au NCs plus αPD-L1, we rechallenged mice with the secondary CT26 tumors after 40 days of the first tumor removed by different treatments or surgery. In details, mice were divided into four groups (n = 5 per group) (Group 1, Surgery; Group 2, Surgery plus αPD-L1 (pre and post); Group 3, ^{177}Lu@Au NCs (i.t.) plus αPD-L1 (pre); Group 4, ^{177}Lu@Au NCs (i.t.) plus αPD-L1 (pre and post)) and αPD-L1 was injected at day 1, 3, 5 (pre injection) and day 41, 43 and 45 (post injection) respectively (Fig. 6a). For mice treated their first tumors by surgery, the growth of re-challenged tumors exhibited no significant inhibition even injected with two rounds αPD-L1 (pre and post) (Fig. 6b). However, for mice with their first tumors removed by ^{177}Lu@Au NCs plus αPD-L1 (pre) or ^{177}Lu@Au NCs plus αPD-L1 (pre and post), no tumor growth was found after rechallenged with the secondary tumors, indicating the long-term immune protective effect induced by ^{177}Lu@Au NCs plus αPD-L1(Fig. 6c). To study the mechanisms of immune memory effect induced by radio-immunotherapy of ^{177}Lu@Au NCs, central memory T cells (T_{CM}), and effector memory T cells (T_{EM}) in the spleen were analysed by flow cytometry assay at day 40. Notably, it was observed that the percentage of T_{EM} cells ($CD3^+CD8^+CD62L^-CD44^+$), which could give rise to immediate immune protections *via* generating cytokines, exhibited prominently increase in ^{177}Lu@Au NCs plus αPD-L1 group compared to other groups (Fig. 6d). Moreover, TNF-α and IFN-γ showed obvious increase in serum through ELISA kits assay (Fig. 6e). Those results obviously indicated that the immune memory effect induced by our treatment strategy could protect organisms from a second wave of tumor cells infection.

Internal radioisotope therapy plus immunotherapy for transgenic mice with spontaneous and metastatic cancer

To further evaluate the promise of our strategy for clinical cancer treatment, ransgenic mice with spontaneous breast tumors, which are more similar to human tumors than subcutaneous tumor model, were then introduced to evaluate the effectiveness of radio-immunotherapy, which is conducive to pushing the results of animal

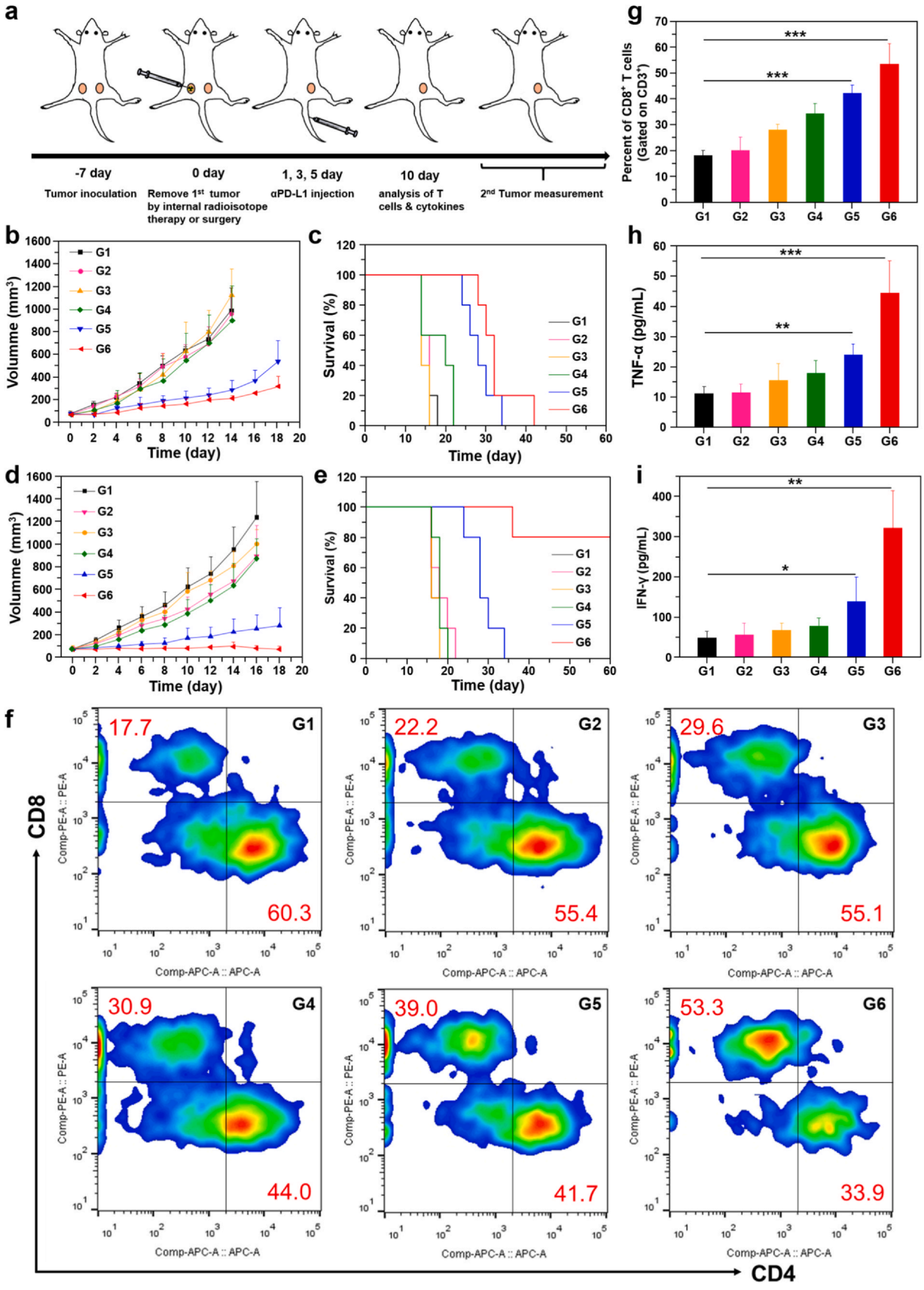

Fig. 5. Distant tumor inhibition by radioimmunotherapy. a) Schematic diagram of local internal radioisotope therapy plus αPD-L1 to suppress distant tumor growth. b) and c) Distant tumor growth curves and survivorship curves of 4T1 tumor-bearing mice after various treatments. d) and e) Distant tumor growth curves and survivorship curves of CT26 tumor-bearing mice after various treatments. Error bars represent mean ± s.d. (n = 5). 4T1 tumor-bearing mice. Error bars represent mean ± s.d. (n = 5). f) Representative flow cytometry plots showing different types of T cells in the secondary tumors from different groups 10 days post treatment (CT26 tumor model). g) Proportions of tumor-infiltrating CD8+ killer T cells among CD3+ cells (CT26 tumor model). Error bars represent mean ± s.d. (n = 4). h) and i) TNF-α level (h) and interferon-γ (IFN-γ) level (i) in mice sera isolated 10 days post various treatments (CT26 tumor model). Error bars represent mean ± s.d. (n = 5). (G1: Surgery, G2: Surgery + αPD-L1, G3: ^{99m}Tc@Au NCs (i.t.), G4: ^{177}Lu@Au NCs (i.t.), G5: ^{99m}Tc@Au NCs (i.t.) + αPD-L1, G6: ^{177}Lu@Au NCs (i.t.) + αPD-L1). P values in (g), (h) and (i) were calculated by multiple *t*-tests (***P < 0.001, **P < 0.01, *P < 0.05).

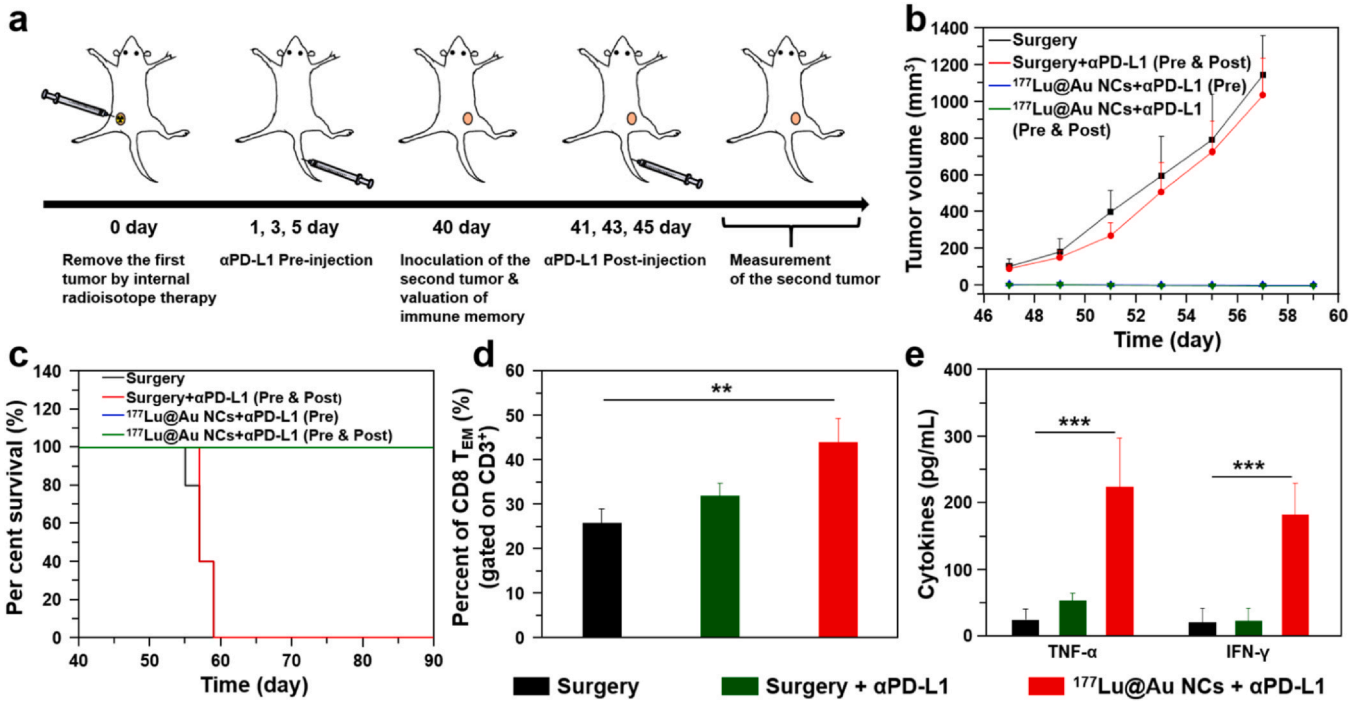

Fig. 6. Immune memory effect of radio-immunotherapy (CT26 tumor model). a) Schematic diagram of immune memory effect by ^{177}Lu@Au NCs (i.t.) plus αPD-L1. b) and c) Tumor growth (b) and survivorship curves (c) of mice in rechallenged tumor experiments after 40 days of the first tumors eliminated by surgery, surgery + αPD-L1 and ^{177}Lu@Au NCs (i.t.) + αPD-L1. Five mice per treatment group (n = 5). d) Quantification of proportions of CD8+ effector memory T cells (T_{EM}) gated on CD3+ cells in the spleen analyzed at day 40 before rechallenging mice with secondary tumors. Error bars represent mean ± s.d. (n = 4). e) TNF-α and IFN-γ levels in sera from mice isolated 40 days post different treatments before rechallenging mice with secondary tumors. Error bars represent mean ± s.d. (n = 5). P values in (d) and (e) were calculated by multiple *t*-tests (***P < 0.001, **P < 0.01).

experiments to humans. It needs to be mentioned that once this spontaneously metastatic tumor occurs, there is no way to completely cure it. In our experiments, when the tumors at breast were clearly visible, transgenic mice were divided into 2 groups at random (n = 5 per group) (Group 1, Control; Group 2, ^{177}Lu@Au NCs (i.t.) plus αPD-L1) and the right breast pad of each mouse in Group 2 was i.t. injected with 25 μL ^{177}Lu@Au NCs (^{177}Lu: 100 μCi, Au: 34.08 mg/mL) (Fig. 7a). Afterwards, mice in Group 2 were then i.v. injected with αPD-L1 (20 μg per mouse) at 1, 3 and 5 days. As shown in Fig. 7b, the lifetime of mice treated by ^{177}Lu@Au NCs combined with αPD-L1 blockade was prominently prolonged about two weeks compared to control group. Meanwhile, the body weights were also monitored during such radio-immunotherapy and no appreciable body weight changes of mice were found, indicating no significant side effects for mice with such treated strategy (Fig. S10). In order to find out the details of treatment condition, photos of mice were collected at 14 day post treatment, further indicating significant therapeutic effect of ^{177}Lu@Au NCs (i.t.) plus αPD-L1 (Fig. S11). Moreover, tumor growth and metastasis at transgenic mice were further monitored at 23 day post treatment by Positron Emission Tomography-Computed Tomography (PET/CT) imaging using ^{18}F-fluorodeoxyglucose (^{18}F-FDG), a most common radiolabelled sugar (glucose) molecule tracer. Compared to control group, tumors treated with radio-immunotherapy were much smaller than that of control group (Fig. 7c). Importantly, the number of metastatic lesions were significantly inhibited by our treated strategy. Afterwards, in order to explore the mechanisms of antitumor immune responses, the ratio of CD8+ CTLs was evaluated by flow cytometry assay at day 30 post treatment. Notably, it was found that the percentage of CTLs showed obvious increase in Group 2 even after 30 days of treatment (Fig. 7d), which was up to 34.24% (Fig. 7e), compared to Group 1. By analysing lung tissue sections of mice at different days, we speculated that such a treatment might be prolong the time of tumor lesion metastasis to a certain extent, which could also be reflected in PET/CT imaging (Fig. S12a and b). To sum up, our experimental results indicated that radio-immunotherapy by ^{177}Lu@Au NCs plus αPD-L1 could effectively inhibit the metastatic tumor. Although the transgenic mice were eventually died, our strategy has significantly prolonged the survival time of the mice. Hence, our strategy is promising for delaying the tumor metastasis in clinical treatment, providing more time and possibility for developing potent therapeutic regimen for the cancer patients.

Conclusion

In summary, the metabolizable and low toxicity radionuclide labelled Au NCs developed by this work would provide a new strategy for cancer diagnosis and therapy based on renal clearable gold nanoparticles. Our study adopted a novel and convenient chelating approach to develop ^{99m}Tc@Au NCs and ^{177}Lu@Au NCs with high radiolabeling stability. It is noteworthy that the radionuclide labelled Au NCs not only endow nontherapeutic ^{99m}Tc with the therapeutic function but also improve the efficacy of therapeutic ^{177}Lu *in vitro* and *in vivo*. Besides, we were surprised to find that such internal radioisotope therapy could induce some immune responses. By combining with αPD-L1 blockade, distant tumors were obviously inhibited, which could also produce a long-term immunological memory effect. Especially, to simulate the real cancer occurred in human, transgenic mice with spontaneous breast tumors were for the first time introduced in our experiments. Through radio-immunotherapy by ^{177}Lu@Au NCs plus αPD-L1 blockade, spontaneous and metastatic tumors were effectively inhibited and the lifetime of transgenic mice were significantly prolonged. In general, such radio-immunotherapy strategy we designed could not only provide efficient internal radioisotope therapy for solid tumors but also prominently eliminate the distant tumors. Especially, the living quality and lifetime of transgenic mice with terminal cancer were also improved by our method. For clinical translation, our strategy might

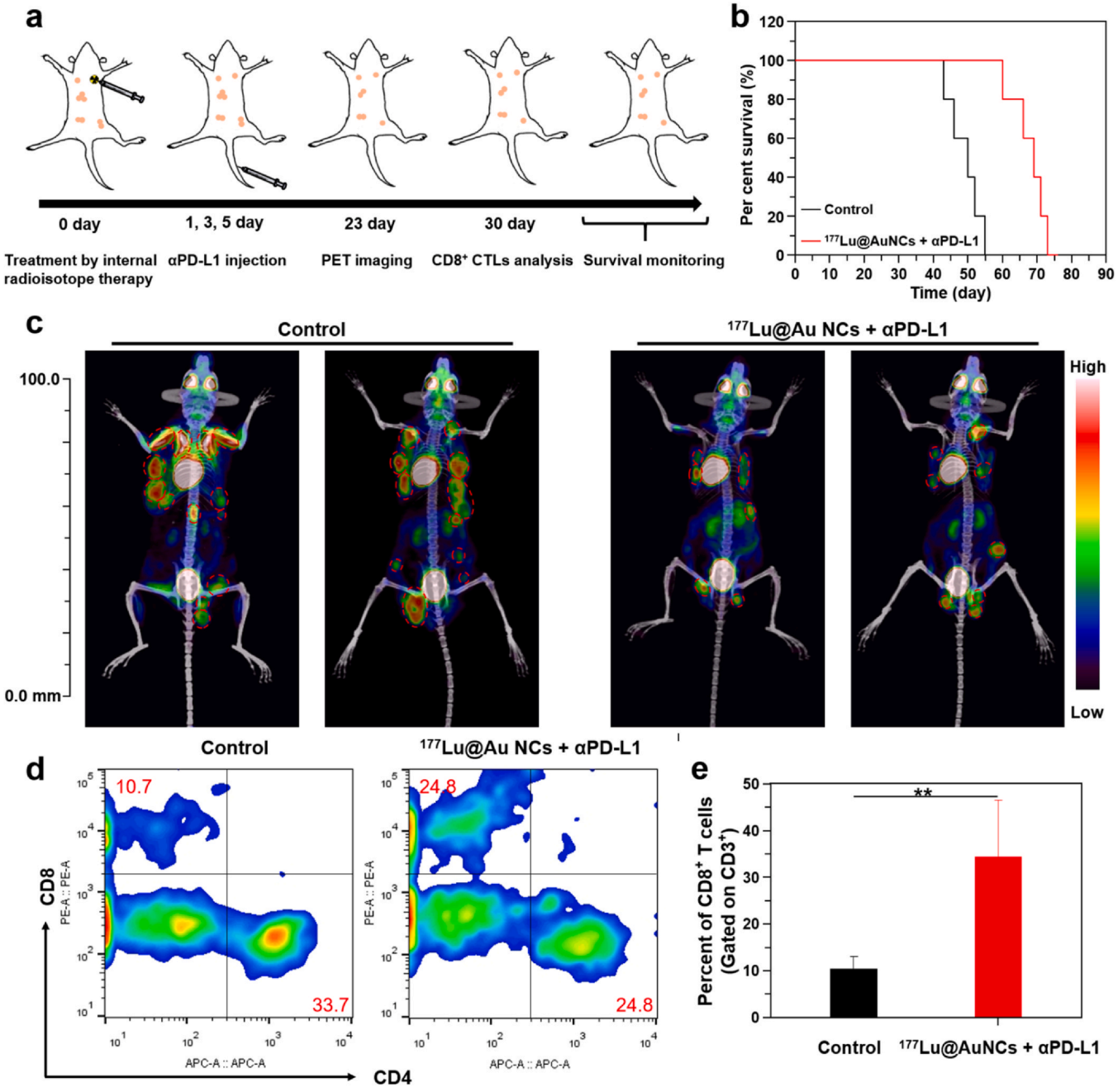

Fig. 7. Transgenic mice (FVB/NJGpt-Tg(MMTV-PyMT)/Gpt) with spontaneous and metastatic breast cancer treated by radio-immunotherapy. a) Schematic diagram of local internal radioisotope therapy plus αPD-L1 to inhibit the growth of spontaneous and metastatic tumors. b) Survival curves of transgenic mice treated by ^{177}Lu@Au NCs (i.t.) + αPD-L1. Five mice per group (n = 5). c) ^{18}F-fluoro-desoxyglucose (FDG) PET/CT images of transgenic mice 23 days post treatment. Two mice per treatment group (n = 2). d) Representative flow cytometry plots showing different types of T cells in solid tumors from transgenic mice in different groups 30 days post treatment. e) Proportions of tumor-infiltrating CD8+ killer T cells among CD3+ cells of transgenic mice. Error bars represent mean ± s.d. (n = 5). P values in (e) were calculated by multiple *t*-tests (**P < 0.01).

have the potential for tumor interventional therapy for many types of solid tumors, such as breast cancer, colon cancer and prostatic cancer. In addition to that, such method may provide more opportunities and time for patients with spontaneously metastatic advanced tumors.

Materials and methods

Materials

Glutathione and $HAuCl_4$ were purchased from Sigma-Aldrich. Anti PD-L1 used *in vivo* was purchased from Bioxcell (Clone: 10F.9G2, Catalog#: BE0101). Antibodies for cell surface markers were obtained from eBioscience. Radioisotope $Na^{99m}TcO_4$ and $^{177}LuCl_3$ were purchased from Shanghai GMS Pharmaceutical Co and ITG ISotope TechnologiES Garching GmbH respectively.

Synthesis of GSH-Au NCs

The GSH-Au NCs was synthesised by chemical reduction method. In details, 150 μL of $HAuCl_4$ solution (1 mol/L) was added to 45 mL of glutathione solution (2.4 mmol/L) in sufficient stirring. Afterwards, the solution was heated to 90 °C for 0.5 h in oil bath. The solution product was cooled to 25 °C and centrifuged at 21,000×*g* to remove

the large aggregates. The solution was then purified by regulating the pH to 3–4, and extracted purified product through aqueous ethanol (2:1, $V_{H2O}/V_{ethanol}$) and 4000×g centrifugation. The precipitate was re-suspended in PBS or water to obtain GSH-Au NCs.

Radioisotope Labelling and labelling stability assay

To perform ^{99m}Tc labelling, 5 mCi of ^{99m}Tc ($Na^{99m}TcO_4$) was firstly mixed with sodium borohydride (50 μL, 5 mg/mL) PBS solution for 5 min and then GSH-Au NCs (1 mL, 34 mg/mL) was added under sufficient stirring at 37 °C for 20 min ^{99m}Tc labelled GSH-Au NCs were then obtained after being purified by ultra-filtration for three times, affording 67.17% labeling yield. Moreover, for ^{177}Lu labelling, 3 mCi of ^{177}Lu ($^{177}LuCl_3$) in 0.05 M hydrochloric acid solution (10 μL) and GSH-Au NCs (1 mL, 34 mg/mL) were mixed under sufficient stirring at 37 °C for 20 min ^{177}Lu labelled GSH-Au NCs were then obtained after being purified by ultra-filtration for three times, affording 90.74% labeling yield.

In order to evaluate radiolabelling stability, radioisotope labelled GSH-Au NCs (^{99m}Tc@Au NCs or ^{177}Lu@Au NCs) were mixed with serum or PBS buffer for 24 h. The solution was sampled to filter through Ultra Centrifugal 10 kDa Filters (Millipore) at different time points. The added radioactivities and radioactivities retained on the filters were detected by gamma counter (PerkinElmer) to evaluate the radiolabelling stability. For liquid scintillation spectrum, 50 μL of GSH-Au NCs, free ^{99m}Tc, ^{99m}Tc@Au NCs, or ^{177}Lu@Au NCs were added in 3 mL PE scintillation liquid (PerkinElmer) and detected by the liquid scintillation analyser (PerkinElmer, Tri-Carb 2910TR).

In vitro experiments

The 4T1 mouse breast cancer cell line (4T1 cells), CT26 mouse colon cancer cell line (CT26) and HUVEC human umbilical vein endothelial cell line (HUVEC) were purchased from Cell Source Center, Chinese Academy of Science (Shanghai, China), respectively. 4T1 cells, CT26 cells and HUVEC cells were cultured with standard condition. For biocompatibility evaluation, different concentration (0–160 μg/mL) GSH-Au NCs were co-cultured with 4T1 cells or HUVEC cells for 24 h, relative cell viabilities were evaluated *via* 3-(4,5-dimethyl-2-thiazolyl)-2,5-diphenyl-2-H-tetrazolium bromide (MTT) assay.

For *in vitro* internal radioisotope therapy studies, free ^{99m}Tc, free ^{177}Lu, ^{99m}Tc@Au NCs and ^{177}Lu@Au NCs (160 μg/mL) cells were c-cultured with 4T1 cells at different radioactive dose (^{99m}Tc: 0, 12.5, 25, 50, 100, 200, and 300 μCi, ^{177}Lu: 0, 0.313, 0.613, 1.25, 2.5, 5, and 10 μCi) for 24 h. Then, the relative cell viabilities were evaluated by MTT assay.

For the clonogenic assay, 4T1 cells were seeded in 6-well plates at densities of 200, 400, 600 and 800 cells per well. Afterwards, cells were incubated with 160 μg/mL of ^{99m}Tc@Au NCs or ^{177}Lu@Au NCs with different radioactive dose (^{99m}Tc: 0, 100, 200, and 300 μCi, ^{177}Lu: 0, 2.5, 5, and 10 μCi) for 24 h. Cells were further cultured for 3–7 days and fixed by 4% paraformaldehyde and then stained *via* crystal violet. The surviving fractions were calculated by the ratio of surviving colonies and seeded cells.

For γ-H2AX staining studies, 4T1 cells were seeded in 6-well plates at densities of 5×10^4 cells/well. After 24 h, cells were treated with 160 μg/mL of ^{99m}Tc@Au NCs or ^{177}Lu@Au NCs at different radioactive dose (^{99m}Tc: 300 μCi, ^{177}Lu: 10 μCi) for 12 h. Another 12 h later, cells were dealt with γ-H2AX and DAPI and imaged by confocal microscopy (Olympus).

Tumor model

Female BALB/c mice (6–8 weeks) were purchased from Changzhou Kavins Experimental Animal Co. LTD. Female FVB/NJGpt-Tg(MMTV-PyMT)/Gpt mice (8 weeks) were purchased from GemPhamatech Co. LTD. The contract information was provided in Supplementary Material (Fig. S13). Animal experiments were performed according to the protocols approved by Soochow University Laboratory Animal Center.

4T1 cells or CT26 colorectal cancer cells (2×10^6) in 50 μL PBS were injected onto the back of BALB/c mouse to build the tumor model. All mice were randomly divided in experiments. Tumor size was calculated by the following formula: volume = (tumor length) × (tumor width)^2/2, mice will be euthanized, when volume of tumors reached above 1000 mm^3.

In vivo experiments

For *in vivo* SPECT imaging and bio-distribution studies, 4T1 tumor-bearing mice were i.v. or i.t. injected with ^{99m}Tc@Au NCs or Free ^{99m}Tc at radioactive dose of 800 μCi and i.t. injected with ^{177}Lu@Au NCs or free ^{177}Lu at radioactive dose of 100 μCi (25 μL, Au: 34.08 mg/mL) and SPECT/CT images were collected by an U-SPECT+/CT imaging system (MILABS) post injection. To investigate bio-distribution of ^{99m}Tc@Au NCs, 4T1 tumor-bearing mice were i.v. or i.t. pre-injected with ^{99m}Tc@Au NCs and Free ^{99m}Tc at radioactive dose of 200 μCi and mice were sacrificed at 24 h post-injection to obtain organs and tumors for radioactivity testing by γ counter.

For subcutaneous tumors inhibition, mice bearing with 4T1 tumors were divided into 7 groups at random (5 mice per group). When the volume of tumor reached ~100 mm^3, mice were injected with PBS, GSH-Au NCs (i.v., 200 μL, Au: 4.26 mg/mL), GSH-Au NCs (i.t., 25 μL, Au: 34.08 mg/mL), Free ^{99m}Tc (i.t., 200 μCi), Free ^{177}Lu (i.t., 75 μCi), ^{99m}Tc@Au NCs (i.v., 400 μCi), ^{177}Lu@Au NCs (i.v., 200 μCi), ^{99m}Tc@Au NCs (i.t., 200 μCi) and ^{177}Lu@Au NCs (i.t., 75 μCi) respectively at 0 day.

For distant tumors inhibition, 4T1 or CT26 cells were inoculated onto both flanks of every BALB/c mouse back. When the volume of both tumors reached ~75 mm^3, mice were divided into 6 groups at random (G1: Surgery, G2: Surgery plus αPD-L1, G3: ^{99m}Tc@Au NCs (i.t.), G4: ^{177}Lu@Au NCs (i.t.), G5: ^{99m}Tc@Au NCs (i.t.) plus αPD-L1, G6: ^{177}Lu@Au NCs (i.t.) plus αPD-L1, 5 mice per group). For right flank tumor, 25 μL ^{99m}Tc@Au NCs (Au: 34.08 mg/mL, ^{99m}Tc: 200 μCi) was injected in G3 and G5, 25 μL ^{177}Lu@Au NCs (Au: 34.08 mg/mL, ^{177}Lu: 75 μCi,) was injected in G4 and G6. However, the therapeutic effect of ^{99m}Tc@Au NCs was limited by short radioactive half-life, which could not eliminate the right flank tumors completely and the tumors were surgically removed latterly if too large. Mice in G2, G5 and G6 were then i.v. injected with αPD-L1 (20 μg per mouse) at 1, 3 and 5 days. After that, the growth of left flank tumors was monitored every two days. Mice were euthanized, when volume of left flank tumors reached above 1000 mm^3.

To study the immune memory effect, CT26 cells were inoculated onto right flanks of every BALB/c mouse. When the volume of tumors both reached about 50 mm^3, the tumors were eliminated by surgery or 25 μL ^{177}Lu@Au NCs (i.t., ^{177}Lu: 75 μCi, Au: 34.08 mg/mL) plus αPD-L1 (20 μg per mouse). 40 days later, when the secondary CT26 tumors were inoculated, αPD-L1 (20 μg per mouse) was i.v. injected into the mice at 41, 43 and 45 days. The size of secondary tumors was measured every two days to monitor survival of mice.

To study transgenic mice treated by internal radioisotope therapy and immunotherapy, when the transgenic mice were 8 weeks old, 25 μL ^{177}Lu@Au NCs (i.t., ^{177}Lu:100 μCi, Au: 34.08 mg/mL) were injected in the tumor under the right breast pad transgenic mice. Afterwards, αPD-L1 was i.v. injected into the transgenic mice at 1, 3 and 5 days. The growth and metastasis of tumors was evaluated by ^{18}F-fluoro-desoxyglucose (FDG) PET/CT imaging (SIEMENS Inveon PET/CT) at 23 days post treatment. Beyond that, survival of transgenic mice was further monitored carefully every day.

Ex vivo analysis of dendritic cells

To study *in vivo* DCs stimulation studies, lymph gland was obtained from the ipsilateral inguinal of each CT26 tumor-bearing mouse 3 days post treatments (Surgery, Free ^{99}mTc, ^{177}Lu, ^{99m}Tc@Au NCs, ^{177}Lu@Au NCs (^{177}Lu: 75 μCi, ^{99m}Tc: 200 μCi)) and homogenized in PBS (pH 7.4) containing 1% Fetal Bovine Serum (FBS) to acquire cell suspension. After that, the DCs were stained by anti-CD11c-FITC (eBioscience, Clone: N418, 11-0114-82), anti-CD86-APC (eBioscience, Clone: GL1, 17-0862-82) and anti-CD80-PE (eBioscience, Clone: 16–10A1, 12-0801-82) antibodies for flow cytometry assay.

Ex vivo analysis of PD-L1 expression on tumor cells

To study PD-L1 expression on distant tumors cells, CT26 tumors were obtained from mice (Surgery, Free ^{99m}Tc, ^{177}Lu, ^{99m}Tc@Au NCs, ^{177}Lu@Au NCs (^{177}Lu: 75 μCi, ^{99m}Tc: 200 μCi)) and homogenized in PBS (pH 7.4) containing 1% FBS to obtain cell suspension. Afterwards, cells were stained by anti-CD3-FITC (eBioscience, Clone: 17A2, 11-0032-82), αPD-L1-PE (eBioscience) antibodies for flow cytometry assay. For immunofluorescence staining, tumor slices were stained with DAPI and αPD-L1-FITC (abcam, [EPR20529], ab213480).

Ex vivo analysis of T cells

To study the T cells in distant tumors or transgenic mice, 4T1 or CT26 tumors were obtained from mice and homogenized in PBS (pH 7.4) containing 1% FBS to acquire cell suspension. To analyse $CD8^+$ T cells, cells was stained by anti-CD3-FITC (eBioscience, Clone: 17A2, 11-0032-82), anti-CD8a-PE (eBioscience, Clone: 53-6.7, 12-0081-83) and antiCD4-APC (eBioscience, Clone: GK1.5, 17-0041-83) antibodies according to protocol to distinguish cytotoxic T lymphocytes (CTLs, $CD3^+CD4^-CD8^+$) and helper T cells ($CD3^+CD4^+CD8^-$). To study memory T cells, spleens were obtained from mice in different groups at 40 days post treatments and stained by anti-CD3-FITC (eBioscience, Clone: 17A2, 11-0032-82), anti-CD8-PE (eBioscience, Clone: 53-6.7, 12-0081-83), anti-CD62L-PE-Cyanine7 (eBioscience, Clone: MEL-14, 25-0621-82) and anti-CD44-APC (eBioscience, Clone: IM7, 17-0441-82) antibodies. Central memory T cells (TCM) and effector memory T cells (TEM) were $CD3^+CD8^+CD62L^+CD44^+$ and $CD3^+CD8^+CD62L^-CD44^+$, respectively.

Cytokine detection

Serum samples were obtained from mice in different groups and diluted for analysis. Tumor necrosis factor (TNF-α, Dakewe biotech) and interferon gamma (IFN-γ, Dakewe biotech) were analysed by ELISA kits according to vendors' instructions.

Statistical analysis

All results are expressed as means ± SEM or SD as indicated. Multiple *t*-tests were used when two groups were compared.

CRediT authorship contribution statement

Kai Yang conceived the project; Pei Pei and Wenhao Shen performed the radiolabeling experiments; Hailin Zhou and Yuanchen Sun carried out SPECT imaging; Jing Zhong carried out the immunological experiment; Teng Liu reviewed the manuscript.

Declaration of Competing Interest

The authors declare that they have no known competing financial interests or personal relationships that could have appeared to influence the work reported in this paper.

Acknowledgements

This work was partially supported by the National Natural Science Foundation of China (31822022, U1932208), a Jiangsu Natural Science Fund for Outstanding Youth Science Foundation (BK20180094), the Postgraduate Research & Practice Innovation Program of Jiangsu Province (KYCX20_2683), the Project Funded by the Priority Academic Program Development of Jiangsu Higher Education Institutions (PAPD).

Appendix A. Supporting information

Supplementary data associated with this article can be found in the online version at doi:10.1016/j.nantod.2021.101144.

References

[1] D.M. Gilkes, G.L. Semenza, D. Wirtz, Hypoxia and the extracellular matrix: drivers of tumour metastasis, Nat. Rev. Cancer 14 (2014) 430–439.
[2] C. Coghlin, G.I. Murray, Current and emerging concepts in tumour metastasis: concepts in tumour metastasis, J. Pathol. 222 (2010) 1–15.
[3] N.K. Altorki, G.J. Markowitz, D. Gao, J.L. Port, A. Saxena, B. Stiles, T. McGraw, V. Mittal, The lung microenvironment: an important regulator of tumour growth and metastasis, Nat. Rev. Cancer 19 (2019) 9–31.
[4] F.J. Esteva, V.M. Hubbard-Lucey, J. Tang, L. Pusztai, Immunotherapy and targeted therapy combinations in metastatic breast cancer, Lancet Oncol. 20 (2019) e175–e186.
[5] W. Yue, L. Chen, L. Yu, B. Zhou, H. Yin, W. Ren, C. Liu, L. Guo, Y. Zhang, L. Sun, K. Zhang, H. Xu, Y. Chen, Checkpoint blockade and nanosonosensitizer-augmented noninvasive sonodynamic therapy combination reduces tumour growth and metastases in mice, Nat. Commun. 10 (2019) 2025–2040.
[6] L. Necula, L. Matei, D. Dragu, A.I. Neagu, C. Mambet, S. Nedeianu, C. Bleotu, C.C. Diaconu, M. Chivu-Economescu, Recent advances in gastric cancer early diagnosis, World J. Gastroenterol. 25 (2019) 2029–2044.
[7] H. Luo, Q. Zhao, W. Wei, L. Zheng, S. Yi, G. Li, W. Wang, H. Sheng, H. Pu, H. Mo, Z. Zuo, Z. Liu, C. Li, C. Xie, Z. Zeng, W. Li, X. Hao, Y. Liu, S. Cao, W. Liu, S. Gibson, K. Zhang, G. Xu, R.H. Xu, Circulating tumor DNA methylation profiles enable early diagnosis, prognosis prediction, and screening for colorectal cancer, Sci. Transl. Med. 12 (2020) eaax7533.
[8] C.A. Klein, Cancer progression and the invisible phase of metastatic colonization, Nat. Rev. Cancer 20 (2020) 681–694.
[9] N. Harbeck, F. Penault-Llorca, J. Cortes, M. Gnant, N. Houssami, P. Poortmans, K. Ruddy, J. Tsang, F. Cardoso, Breast cancer, Nat. Rev. Dis. Prim. 5 (2019) 66.
[10] Q. Wang, H. Peng, X. Qi, M. Wu, X. Zhao, Targeted therapies in gynecological cancers: a comprehensive review of clinical evidence, Signal Transduct. Target Ther. 5 (2020) 137.
[11] C. Gutta, A. Rahman, C. Aura, P. Dynoodt, E.M. Charles, E. Hirschenhahn, J. Joseph, J. Wouters, C. de Chaumont, M. Rafferty, M. Warren, J.J. van den Oord, W.M. Gallagher, M. Rehm, Low expression of pro-apoptotic proteins Bax, Bak and Smac indicates prolonged progression-free survival in chemotherapy-treated metastatic melanoma, Cell Death Dis. 11 (2020) 124–136.
[12] F. Loupakis, H.I. Hurwitz, L. Saltz, D. Arnold, A. Grothey, Q.L. Nguyen, S. Osborne, J. Talbot, S. Srock, H.J. Lenz, Impact of primary tumour location on efficacy of bevacizumab plus chemotherapy in metastatic colorectal cancer, Br. J. Cancer 119 (2018) 1451–1455.
[13] Y.T. Lee, Y.J. Tan, C.E. Oon, Molecular targeted therapy: treating cancer with specificity, Eur. J. Pharmacol. 834 (2018) 188–196.
[14] A.B. Schulze, G. Evers, A. Kerkhoff, M. Mohr, C. Schliemann, W.E. Berdel, L.H. Schmidt, Future options of molecular-targeted therapy in small cell lung cancer, Cancers 11 (2019) 690.
[15] A.B. Shaikh, F. Li, M. Li, B. He, X. He, G. Chen, B. Guo, D. Li, F. Jiang, L. Dang, S. Zheng, C. Liang, J. Liu, C. Lu, B. Liu, J. Lu, L. Wang, A. Lu, G. Zhang, Present advances and future perspectives of molecular targeted therapy for osteosarcoma, IJMS 17 (2016) 506.
[16] J.H. Sampson, M.D. Gunn, P.E. Fecci, D.M. Ashley, Brain immunology and immunotherapy in brain tumours, Nat. Rev. Cancer 20 (2020) 12–25.
[17] J. Nam, S. Son, K.S. Park, W.P. Zou, L.D. Shea, J.J. Moon, Cancer nanomedicine for combination cancer immunotherapy, Nat. Rev. Mater. 4 (2019) 398–414.
[18] N.P. Staff, A. Grisold, W. Grisold, A.J. Windebank, Chemotherapy-induced peripheral neuropathy: a current review: CIPN, Ann. Neurol. 81 (2017) 772–781.
[19] R. Oun, Y.E. Moussa, N.J. Wheate, The side effects of platinum-based chemotherapy drugs: a review for chemists, Dalton Trans. 47 (2018) 6645–6653.

[20] X. Ke, L. Shen, Molecular targeted therapy of cancer: the progress and future prospect, Front. Lab. Med. 1 (2017) 69–75.
[21] U. Sahin, O. Tureci, Personalized vaccines for cancer immunotherapy, Science 359 (2018) 1355–1360.
[22] A. Ribas, J.D. Wolchok, Cancer immunotherapy using checkpoint blockade, Science 359 (2018) 1350–1355.
[23] Y. Chao, C. Liang, H. Tao, Y. Du, D. Wu, Z. Dong, Q. Jin, G. Chen, J. Xu, Z. Xiao, Q. Chen, C. Wang, J. Chen, Z. Liu, Localized cocktail chemoimmunotherapy after in situ gelation to trigger robust systemic antitumor immune responses, Sci. Adv. 6 (2020) eaaz4204.
[24] Y. Chao, L. Xu, C. Liang, L. Feng, J. Xu, Z. Dong, L. Tian, X. Yi, K. Yang, Z. Liu, Combined local immunostimulatory radioisotope therapy and systemic immune checkpoint blockade imparts potent antitumour responses, Nat. Biomed. Eng. 2 (2018) 611–621.
[25] Y. Chao, C. Liang, Y. Yang, G. Wang, D. Maiti, L. Tian, F. Wang, W. Pan, S. Wu, K. Yang, Z. Liu, Highly effective radioisotope cancer therapy with a non-therapeutic isotope delivered and sensitized by nanoscale coordination polymers, ACS Nano 12 (2018) 7519–7528.
[26] P.S. Hegde, D.S. Chen, Top 10 challenges in cancer immunotherapy, Immunity 52 (2020) 17–35.
[27] W. Song, S.N. Musetti, L. Huang, Nanomaterials for cancer immunotherapy, Biomaterials 148 (2017) 16–30.
[28] R. Timmerman, R. Paulus, J. Galvin, J. Michalski, W. Straube, J. Bradley, A. Fakiris, A. Bezjak, G. Videtic, D. Johnstone, J. Fowler, E. Gore, H. Choy, Stereotactic body radiation therapy for inoperable early stage lung cancer, JAMA 303 (2010) 1070–1076.
[29] G. Song, L. Cheng, Y. Chao, K. Yang, Z. Liu, Emerging nanotechnology and advanced materials for cancer radiation therapy, Adv. Mater. 29 (2017) 1700996.
[30] C. Liang, Y. Chao, X. Yi, J. Xu, L. Feng, Q. Zhao, K. Yang, Z. Liu, Nanoparticle-mediated internal radioisotope therapy to locally increase the tumor vasculature permeability for synergistically improved cancer therapies, Biomaterials 197 (2019) 368–379.
[31] J.J. Liu, Q. Chen, L.Z. Feng, Z. Liu, Nanomedicine for tumor microenvironment modulation and cancer treatment enhancement, Nano Today 21 (2018) 55–73.
[32] J. Zhao, M. Zhou, C. Li, Synthetic nanoparticles for delivery of radioisotopes and radiosensitizers in cancer therapy, Cancer Nanotechnol. 7 (2016) 9.
[33] X. Yi, M. Xu, H. Zhou, S. Xiong, R. Qian, Z. Chai, L. Zhao, K. Yang, Ultrasmall hyperbranched semiconducting polymer nanoparticles with different radioisotopes labeling for cancer theranostics, ACS Nano 12 (2018) 9142–9151.
[34] J. Jeon, Review of therapeutic applications of radiolabeled functional nanomaterials, IJMS Sci. 20 (2019) 2323.
[35] B. Yu, H. Wei, Q. He, C.A. Ferreira, C.J. Kutyreff, D. Ni, Z.T. Rosenkrans, L. Cheng, F. Yu, J.W. Engle, X. Lan, W. Cai, Efficient uptake of177Lu-porphyrin-PEG nanocomplexes by tumor mitochondria for multimodal-imaging-guided combination therapy, Angew. Chem. Int. Ed. 57 (2018) 218–222.
[36] L. Tian, Y. Wang, L. Sun, J. Xu, Y. Chao, K. Yang, S. Wang, Z. Liu, Cerenkov luminescence-induced NO release from 32P-labeled ZnFe(CN)5NO nanosheets to enhance radioisotope-immunotherapy, Matter 1 (2019) 1061–1076.
[37] L. Tian, X. Yi, Z. Dong, J. Xu, C. Liang, Y. Chao, Y. Wang, K. Yang, Z. Liu, Calcium bisphosphonate nanoparticles with chelator-free radiolabeling to deplete tumor-associated macrophages for enhanced cancer radioisotope therapy, ACS Nano 12 (2018) 11541–11551.
[38] Y. Zhang, Q. Wang, G. Chen, P. Shi, DNA-functionalized metal–organic framework: cell imaging, targeting drug delivery and photodynamic therapy, Inorg. Chem. 58 (2019) 6593–6596.
[39] X. Bai, Y. Wang, Z. Song, Y. Feng, Y. Chen, D. Zhang, L. Feng, The basic properties of gold nanoparticles and their applications in tumor diagnosis and treatment, IJMS 21 (2020) 2480.
[40] J. Yang, T. Wang, L. Zhao, V.K. Rajasekhar, S. Joshi, C. Andreou, S. Pal, H.T. Hsu, H. Zhang, I.J. Cohen, R. Huang, R.C. Hendrickson, M.M. Miele, W. Pei, M.B. Brendel, J.H. Healey, G. Chiosis, M.F. Kircher, Gold/alpha-lactalbumin nanoprobes for the imaging and treatment of breast cancer, Nat. Biomed. Eng. 4 (2020) 686–703.
[41] R. Shukla, N. Chanda, A. Zambre, A. Upendran, K. Katti, R.R. Kulkarni, S.K. Nune, S.W. Casteel, C.J. Smith, J. Vimal, E. Boote, J.D. Robertson, P. Kan, H. Engelbrecht, L.D. Watkinson, T.L. Carmack, J.R. Lever, C.S. Cutler, C. Caldwell, R. Kannan, K.V. Katti, Laminin receptor specific therapeutic gold nanoparticles (198AuNP-EGCg) show efficacy in treating prostate cancer, Proc. Natl. Acad. Sci. 109 (2012) 12426–12431.
[42] R. Chakravarty, S. Chakraborty, A. Guleria, R. Shukla, C. Kumar, K.V. Vimalnath Nair, H.D. Sarma, A.K. Tyagi, A. Dash, Facile one-pot synthesis of intrinsically radiolabeled and cyclic RGD conjugated199Au nanoparticles for potential use in nanoscale brachytherapy, Ind. Eng. Chem. Res. 57 (2018) 14337–14346.
[43] S. Yook, Z. Cai, Y. Lu, M.A. Winnik, J.P. Pignol, R.M. Reilly, Radiation nanomedicine for EGFR-positive breast cancer: panitumumab-modified gold nanoparticles complexed to the β-particle-emitter,177Lu, Mol. Pharm. 12 (2015) 3963–3972.
[44] C. Zhou, G. Hao, P. Thomas, J. Liu, M. Yu, S. Sun, O.K. Oz, X. Sun, J. Zheng, Near-infrared emitting radioactive gold nanoparticles with molecular pharmacokinetics, Angew. Chem. Int. Ed. 51 (2012) 10118–10122.
[45] C. Zhou, M. Long, Y. Qin, X. Sun, J. Zheng, Luminescent gold nanoparticles with efficient renal clearance, Angew. Chem. Int. Ed. 50 (2011) 3168–3172.
[46] J. Liu, M. Yu, C. Zhou, S. Yang, X. Ning, J. Zheng, Passive tumor targeting of renal-clearable luminescent gold nanoparticles: long tumor retention and fast normal tissue clearance, J. Am. Chem. Soc. 135 (2013) 4978–4981.
[47] M. Yu, J. Xu, J. Zheng, Renal clearable luminescent gold nanoparticles: from the bench to the clinic, Angew. Chem. Int. Ed. 58 (2019) 4112–4128.
[48] W. Su, C. Chen, T. Wang, X. Li, Y. Liu, H. Wang, S. Zhao, C. Zuo, G. Sun, W. Bu, Radionuclide-labeled gold nanoparticles for nuclei-targeting internal radio-immunity therapy, Mater. Horiz. 7 (2020) 1115–1125.